Design and Optimization of a Multimode Amphibious Robot with Propeller-leg

Xinmeng Ma*, *Student Member, IEEE*, Gang Wang†, *Member, IEEE*, Kaixin Liu*

***Abstract*—This paper describes the design, optimization, and performance evaluation of a novel multimode motion robot named SHOALBOT, which with multimode operations depends on only one type of propulsion device and can work flexibly in the amphibious environment include running on beaches, grasslands, seabed, and swimming in the water. Robots that work in water need to minimize the number of drive components to improve reliability and reduce communication pressure, our unique design enables the robot to rely on a kind of propulsion device named propeller-leg to have the ability to run rapidly in the seaside and seabed, and swim with multi degrees of freedom in the water (such a propulsion system contains only four driving elements), and it can make the robot complete more work content and improve its adaptability to the environment. Running is more stable than swimming and will not disturb the animals in the water, but when the robot encounters a high obstacle with a large area coverage, switching the motion mode to the swimming mode can pass directly over obstacles instead of detouring or giving up work, this can improve work efficiency. We analyzed and optimized propeller-leg by simulation combined with the open water test, the propeller-leg's thrust in the water before and after optimization differs by 400% according to the test results. We optimized the minimum difference between the forward and reverse thrust of the propeller-leg to improve the stability of the robot movement process, and optimized the difference from 25% to 3%. This paper provides sufficient technical details and completeness, and through a series of performance evaluation experiments validated that the SHOALBOT has excellent movement ability in the amphibious environment compared to other published amphibious robots of the same size.**

***Index Terms*—Amphibious robot, multimode motion, mechanisms, propeller-leg optimization, shoal environment.**

I. Introduction

ADVANCEMENT in robotics can promote human exploration of nature. Robots can be a valuable tool for collecting scientific data, particularly in harsh and inaccessible locations, such as for mapping the underside of an iceberg using a modified underwater glider [1] as well as monitoring and inspecting freshwater ecosystems [2]. An increasing number of examples have proved that robots can complete tasks in certain specific environments, such as monitoring and mapping the seabed [3]-[5], researching glaciers and icebergs [1], [6], observing biological species [7], collecting biological and geological samples [8], achieving marine rescue [9], and protecting environments [10].

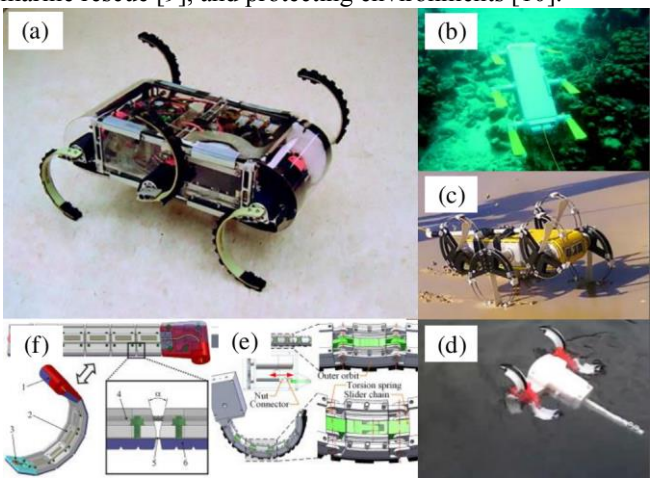

Fig. 1 RHex and the amphibious robots inspired by it. (a) is the RHex with six half-circle legs (from [16]), (b) is the AQUA with six fins as the propulsion device (from [12]), (c) shows the Ninja leg combines the fin and the whole-circle leg (from [20]), (d) shows the robot propulsion device that the mode can be switched between the wheel and the leg through a deformance (from [21] and [22]), (e) (from [24]) and (f) (from [23]) are all use additional mechanisms to enable the robot's propulsion device to switch between fin and half-circle leg.

Amphibious robots have wide application prospects in the fields of security, industry, defense, and transportation because they have several advantages such as efficient obstacle negotiation, strong maneuverability, and a rapid land-water transition [11], [12]. At present, one of the most popular amphibious robot solutions by researchers is the RHex [13]-[17] which exhibits excellent running ability in the amphibious environment relies on six half-circle legs, as few motors as possible to improve the reliability of the robot in the amphibious environment and reduce the complexity of the robot. The characteristics of the half-circle leg such as

*These authors contributed equally to this work. †**Corresponding author. Email: wanggang@hrbeu.edu.cn**

This work was supported in part by the National Natural Science Foundation of China (Grant No. 51779059), in part by the National Natural Science Foundation of Heilongjiang Province (Grant No. YQ2020E028).

Xinmeng Ma, Gang Wang, and Kaixin Liu are with the Science and Technology on Underwater Vehicle Laboratory, Harbin Engineering University, Harbin 150001, China (e-mail:mxm2012071615@hrbeu.edu.cn; liukaixin@hrbeu.edu.cn).

cushioning, climbing, and larger pedaling area, enable the robot to better cope with the soft ground in the amphibious environment, the fly in the ointment is the poor swimming ability of RHex.

Many research institutions have developed various amphibious robots inspired by RHex's design ideas as shown in Fig. 1, and strive to make the robots have more powerful capabilities through more designs while absorbing the expertise of RHex. The AQUA robot changed its half-circle legs to fins, although it improved the swimming ability, the decrease in running ability is obviously [18], [19]. The design of Ninja legs transforms the half-circle legs into whole-circle legs and adds fins to make the robot have the ability to run and swim, but it can be seen that the loss of running ability is serious when the circular legs crawl on the beach ground from the public video, and large deviations of movement will occur when impacted by water currents [20]. Yoo-Seok Kim designed a Wheel-Leg propulsion device that can switch modes between curved legs and wheels, but it can only swim on the surface of the water and has no the ability of multi degrees of freedom swimming in the water [21], [22]. Xu Liang [23] and Long Bai [24] added deformation mechanisms to the half-circle leg to make it has the ability to switch between the half-circle legs and fins in different ways, but the complexity of the system increases, the probability of malfunction of robots working in water increases geometrically with the increase of driving components. The difficulty of underwater communication is much higher than that of land, the demand for communication bandwidth by too many drive components will undoubtedly increase the pressure of communication. In addition, this modification reduces the load capacity and buffer capacity of the half-circle leg.

The energy they can carry is precious for field robots. The load that robot carries higher, the energy consumption faster during the land running. Therefore, the original intention of designing the amphibious robot is to make the robot have swimming ability without adding extra burden.

The contribution of this paper is to propose a new type of robot scheme. Inspired by the RHex robot, aiming at the drawback of its insufficient swimming ability, the amphibious multi-modal robot named SHOALBOT is obtained through the design of the scheme. Relying on the propeller-leg combined with body deformation ability, SHOALBOT not only can run flexibly on the amphibious complex ground but also has the ability to swim by six degrees of freedom in the water, realizes the expansion of motion capabilities from two-dimensional space to three-dimensional space, which allows the robot to have multi-modal motion capabilities in the shoal amphibious environment including grass, beach, water, and seabed. Fig. 2 depicts SHOALBOT's typical working environment, conceptual sketches, and actual working conditions in the amphibious environment. We combined the theories, experiments, simulations, and other methods to complete the design, analysis, and optimization process of SHOALBOT, and optimize the propeller-leg in three aspects, including the maximum thrust, the minimum difference in thrust during forward and reverse rotation, and the friction in running mode. It is verified that this optimized new type of robot scheme has obvious advancement compared with the same size and the same field of robots in terms of movement ability through a series of performance evaluation experiments.

The remaining of the article is structured as follows. In Section II, the multimode operation approach and issues affecting the performance of the propeller-leg are discussed, along with their solutions. In Section III, the modeling and movement simulation of the robot are presented. In Section IV, performance evaluation experiments conducted in a pool and at the seaside are discussed and the abilities achieved by the robot are presented, along with the performance indicators. Finally, in Section V, the conclusions of this article are presented.

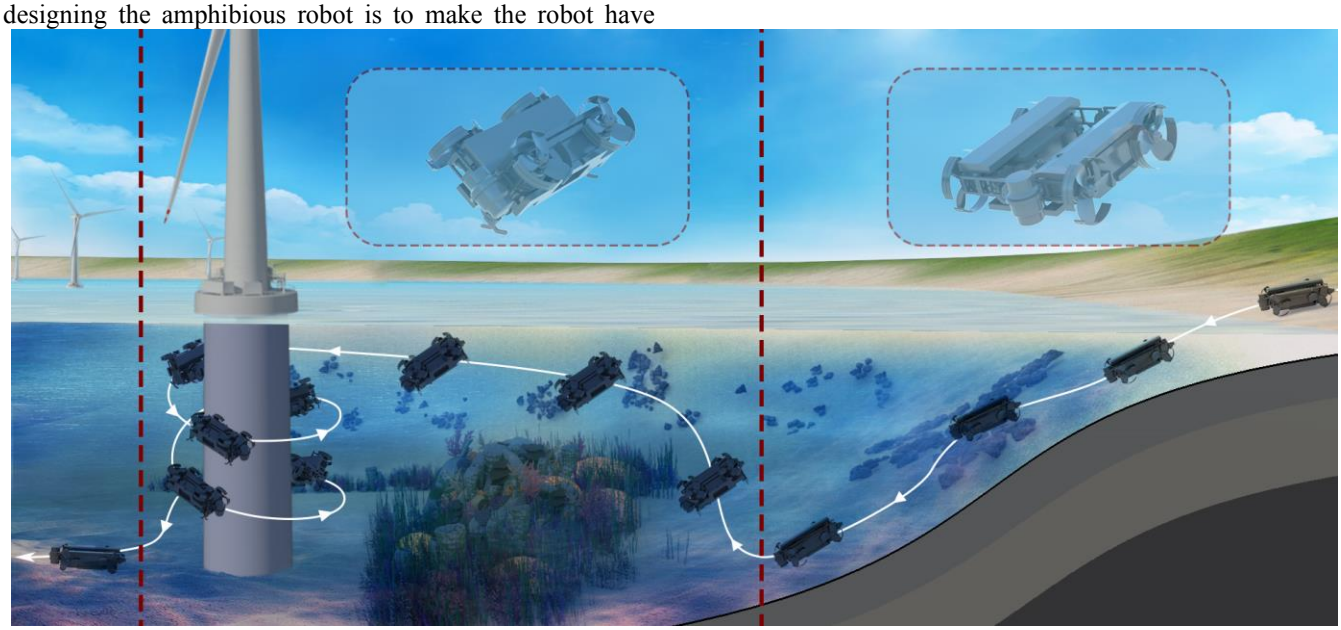

Fig. 2 The typical working environment and working status. The scene shown in the figure is only an example of tasks that the robot can complete, not all.

II. Propeller-leg Mechanism for Multimode Operation in Amphibious Environments

A. Multimode Operation Approach

Fig. 3 shows the main components and operation modes of SHOALBOT. This robot can adapt to complex and changeable amphibious environments more easily using the propulsion ability of the propeller-leg and the deformability of the body. For example, when the robot encounters large areas of coral reefs, direct contact between the robot body and coral reefs when running will damage the natural environment. Moreover, the passage is impossible even if the robot wants to pass the area and detours will significantly decrease the operational efficiency. Thus, the body should be folded to allow the propeller-leg to rotate at high speed to generate axial thrust, thereby enabling flexible swimming in water.

For robots working in water, wireless communication is difficult. SHOALBOT can come near the water surface (depth ~ 15mm), at this time, the 30mm antenna carried by the robot can extend out of the water surface to receive navigation and communication signals. This is the characteristic of the multi-modal robot, it can receive wireless signals when working in the water, compared to the robot that can only crawl at the bottom of the sea, and there is no need to arrange numerous base stations in the water. This characteristic of SHOALBOT is conducive to multiple tasks and communication.

The propeller-leg uses a propeller as the leg and has evenly arranged arc-shaped feet on the edge, facilitate SHOALBOT an excellent running ability of legged robots and the swimming ability of traditional automatic underwater vehicles. Compared with wheeled robots, when SHOALBOT runs, its feet make effective contact with the ground three times during each movement cycle (i.e., the propeller-leg performs a rotate equivalent to 2π), allowing the implementation of more complex control strategies compared with the wheel. Nevertheless, designing the propeller-leg with an operational ability that meets the expected indicators is crucial. Thus, detailed investigations such as hydrodynamic performance analysis, structural scheme selection, and parameter optimization of the propeller-leg are meaningful. In the following subsections, the problems and solutions associated with the three key steps of the propeller-leg solution are discussed.

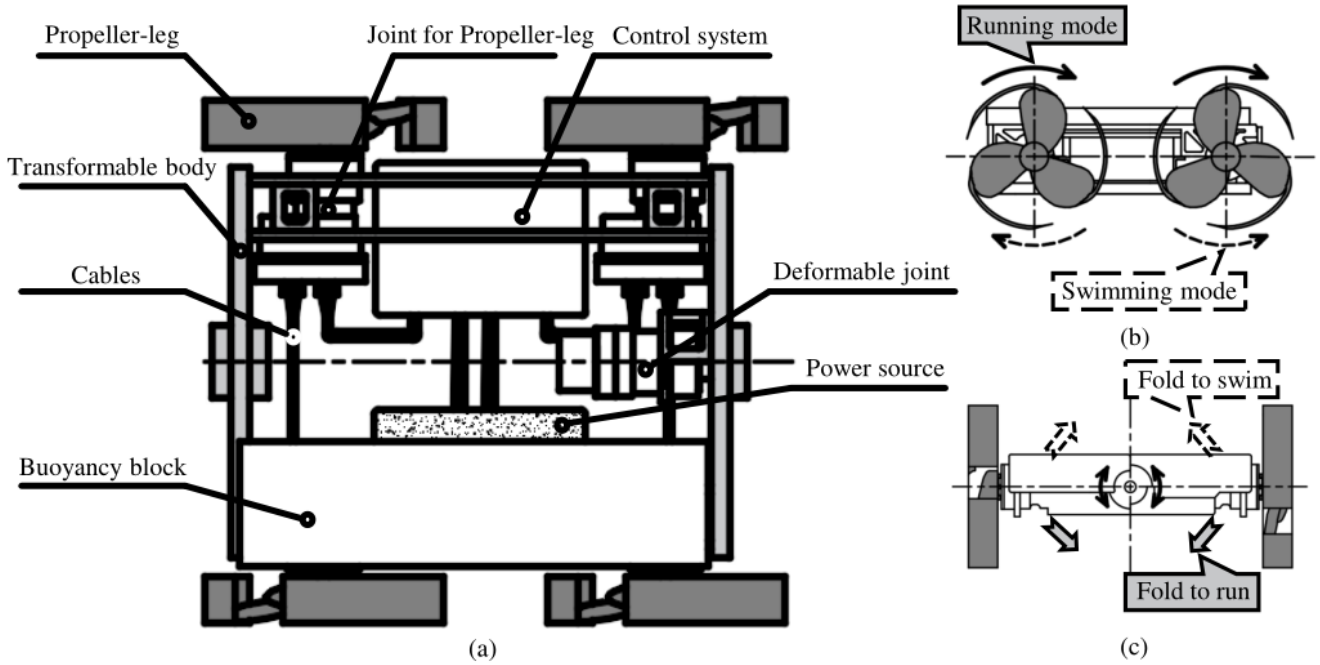

Fig. 3 Main parts and work modes of the SHOALBOT.

B. Step 1: Establish a Simulation Environment for Propeller-leg

Various theories of propeller design are already available; however, these theories are not the focus of our research. For this study, we referred to the Dutch B-series propeller map which is currently widely used. We selected the B3-50 propeller map with a disk ratio of 50% as a reference because the designed propeller will serve as the foundation of the propeller-leg structure, will bear large force so it needs to be strong, therefore, the relevant parameters of the propeller are designed based on B3-50. The final design parameters of the propeller are presented in Table I.

TABLE I
Propeller Parameters

Parameter	Sign	Unit	Value(s)
Diameter	D	mm	220
Pitch ratio	P/D	—	0.48
Type	—	—	B-type Map Propeller
Blade-number	Z	—	3
Disk ratio	AE/A0	—	0.51
Trim angle	E	°	16
Design speed	v	m/s	1.1
Material	—	—	Carbon fiber T700
Weight	G	g	212g

No theoretical calculation model exists that can be used to analyze the propeller-leg; therefore, it is necessary to study the influence of the structural parameters on the propeller-

leg's hydrodynamic characteristics to be optimized. Thus, we must conduct numerous hydrodynamic characteristic tests on the propeller-leg using different structural parameters. However, the cycle time is excessively long as we must fabricate numerous propeller-legs for testing in a circulating water channel if we entirely rely on experimentation. Therefore, we employed simulation methods using the software. We conducted an open water test on the propeller-leg using a set of structural parameters in a circulating water channel and established a simulation environment based on the test results to achieve more accurate simulation results. Table II shows the types of equipment used in the experiment.

TABLE II
EQUIPMENTS OF THE OPEN WATER EXPERIMENT

Equipment	Model
Force sensor	ATI Gamma IP68
Motor	KOLLMORGEN TBM(S)-6013-A
Encoder	RLS MRA029BC010DSE00
Driver	G-SOLTWI15/100EE1
Circulating water channel	Length-7 m, Width-1.7 m, Depth-1.5 m

The force sensor collected data at 50 Hz and processed the obtained discrete data using locally weighted scatterplot smoothing. Fig. 4 shows the test results for a propeller-leg with an arc length and width of 175 mm and 42 mm, respectively. The maximum thrust generated at each flow speed in the experimental results is compared with that in the simulation results. The comparison results are presented in Fig. 4 and Table III.

We use the software Simcenter STAR-CCM+ 2020.2.1 (15.04.010-R8) to complete the simulation work. The simulation adopts the MRF (Moving Reference Frames) method, a rotating area is set around the propeller-leg, and a static flow area is set outside the rotating area. The drainage area is set as a cylinder with a length of 1600mm and a diameter of 1200mm, and the axis of the propeller-leg coincides with the axis of the cylinder. It is found that the wake generated by the propeller has the greatest impact on the simulation results according to the comparison of the open water test and preliminary simulation results, so the mesh at the wake is refined to improve the accuracy of simulation results.

The simulation grid is divided by Tetrahedral cell, reducing the grid size will improve the simulation accuracy, but it will reduce the calculation speed and thus reduce the efficiency of the simulation process. Moreover, it is meaningless to adjust all the grids to a small size, because the grid size of some areas will not affect the simulation accuracy, such as the outer non-enriched part. So the maximum grid size of the outer non-enriched part is 50mm, and the grid size around the propeller-leg and the wake-intensive part is 15mm. A transition part is set between the encrypted and non-encrypted parts, and it slowly transitions from 15mm to 50mm at a rate of 1.3 times for each layer of mesh. At the same time, five boundary layers with a thickness of 1mm are set around the wall of the propeller-leg to ensure the accuracy of the calculation. All the sets of simulations use the same grid parameters to ensure that the simulations have relative accuracy.

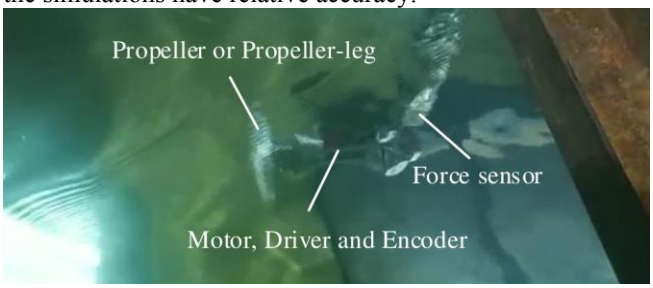

(a)

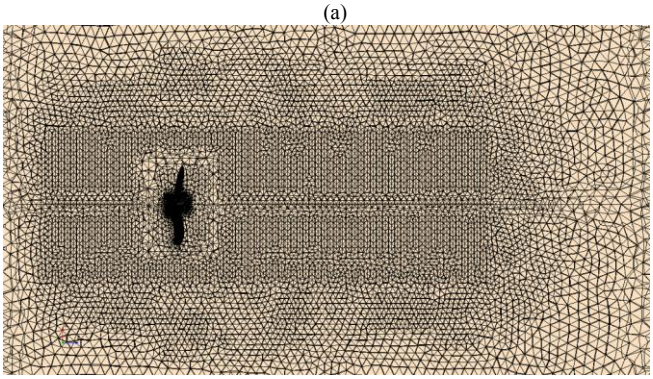

(b)

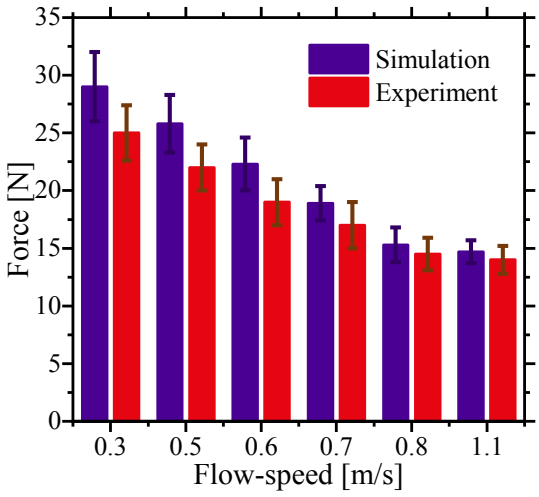

(c)

Fig. 4 Results of the open water experiment and simulation. (a) shows the open water test and data collection in the circulating water channel. (b) shows the meshing during simulation. (c) shows the comparison of the average value of data collected from simulation and experiment. Force is used to represent the propulsion of the propeller-leg and propeller in this paper.

TABLE III
EXPERIMENTAL AND SIMULATION RESULTS

Flow-speed (m/s)	Average of simulation results (N)	Average of experimental results (N)	Error
0.3	29.0	25.0	13.8%
0.5	25.8	22.0	14.7%
0.6	22.3	19.0	14.8%
0.7	18.9	17.0	10.1%
0.8	15.3	14.5	5.2%
1.1	14.7	14.0	4.8%

The comparison analysis indicates that the error is between 4.8% and 14.8%, proving that the simulation results are

consistent with the actual situation; therefore, the simulation results can be used as a reference. Because there is no attachment such as joint and sensor behind the propeller-leg during the simulation process, the turbulence model used has errors, as is inevitable, and the simulation results are slightly larger than the experimental results.

C. Step 2: Analysis of the Propeller-leg's Hydrodynamic Characteristics and Structural Scheme Selection

There are two arrangements of the foot with a direction similar or opposite to the leading edge are proposed. We conducted the simulation and analysis of the two structures and the hydrodynamic performance of the original blade at different rotate-speeds and water flow speeds to investigate the influence of the two arrangements on the hydrodynamic performance. The simulation process and results are shown in Fig. 5. According to the simulation results, the two structures can produce effective thrust when the speed exceeds 200 rpm. However, the thrust of the forward propeller-leg is significantly greater than that of the backward propeller-leg. The thrust comparison shown in Fig. 5(d) indicates that when the speed exceeds 400 rpm and the flow speed is less than 0.6 m/s, the propulsion force generated by the forward propeller-leg is approximately five times that generated by the backward propeller-leg. We processed the propeller and two kinds of propeller-leg by 3D-print technology and carried out verification tests in the circulating water channel, the results are consistent with the simulation results as shown in Fig. 5, which proves that the simulation results are credible. The advantage of the forward propeller-leg is undeniable; hence, the structure of the forward propeller-leg is selected.

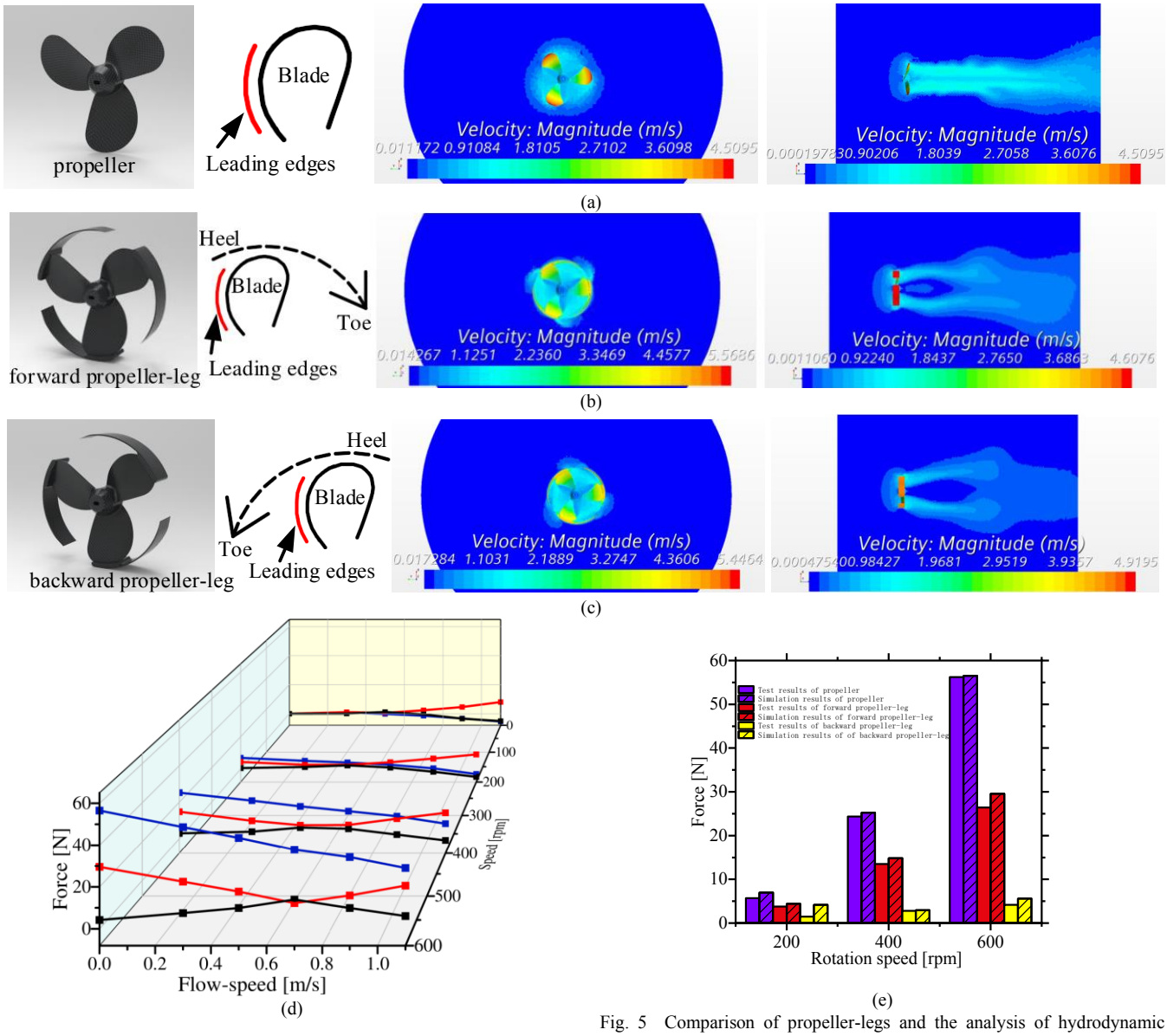

Fig. 5 Comparison of propeller-legs and the analysis of hydrodynamic characteristics. (a), (b) and (c) are the propeller and two structures of propeller-leg. (d) shows the simulation results of the average value of the thrust produced by the three propulsion devices at different flow-speed and rotate-speed, (e) shows the verification of the simulation results in the circulating water channel.

D. *Step 3: Parameter Optimization of the Feet*

After determining the structure of the propeller-leg, the influence of the structural parameters of the arc-shaped feet on the hydrodynamic characteristics was studied. The effect of the foot length and width on hydrodynamic performance was evaluated via simulation analysis. The simulation analysis was conducted under a flow speed of 0 m/s and a rotation speed of 600 rpm, and the analysis results are presented in Fig. 6.

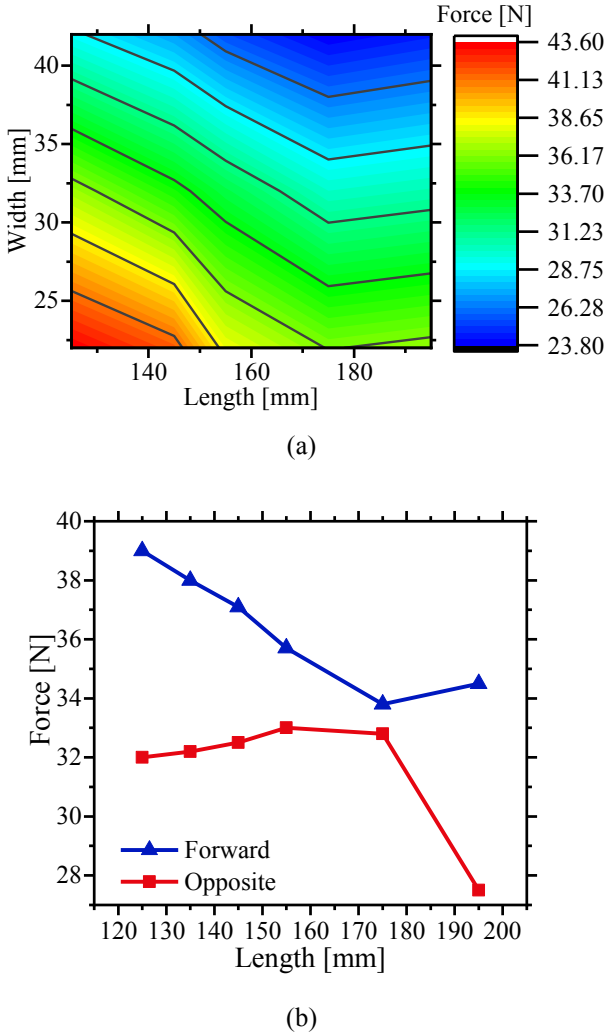

Fig. 6 The simulation results of (a) the effect of the foot length and width on the hydrodynamic characteristics when the propeller-leg rotates at the speed of 600 rpm by the flow-speed is 0 m/s. (b) shows the average value of thrust generated during forward and opposite rotation when the rotate-speed is 600 rpm and the flow-speed is 0 m/s, the difference in force between the dotted lines is the smallest.

It can be seen that the thrust first decreases and then increases as the foot length increases when the propeller-leg forward rotated from Fig. 6(a). As the foot width increases, the thrust gradually decreases. According to the operational requirements, the foot width cannot be less than the axial size of the blade; otherwise, the blade will be damaged when running. Thus, the foot width should be 42 mm. When SHOALBOT is swimming, it must rely on the forward and reverse rotations of each propeller-leg to generate forces in different directions. To reduce the difficulty in controlling the posture during motion and increase the robot's stability when swimming, the thrust difference in the design is assumed to be the smallest in the case of forward and reverse rotations. Therefore, the hydrodynamic characteristics of the forward and reverse rotations with different foot lengths under a 0-m/s flow-speed and 600-rpm rotation speed are analyzed. We optimized the parameters using the minimum thrust difference in the case of forward and reverse rotations as the optimization index. The analysis results are presented in Fig. 6(b). The thrust difference is found to be the smallest (approximately 2.86%) when the foot length is 175 mm.

For optimizing the feet in terms of running ability, set friction as the main optimization index. The method shown in Fig. 7 is adopted to increase the friction without affecting the torque and propulsion in water as much as possible, and a semicylindrical rubber strip is added to the outside of the foot. Experiments and simulations were performed on the propeller-leg to test the influence of different numbers of rubber strips, namely, zero, two, three, four, five, and six rubber strips, on the friction, torque, and hydrodynamic performance.

A friction test device was built (Fig. 7(d)), the ground of different materials can be replaced, such as ABS, wood, aluminum alloy, and so on, it is found that the aluminum alloy material has the smallest surface change with repeated experiments, and the conditions between multiple experiments are the most uniform, so we show the experimental data that tested on the aluminum alloy ground in Fig. 7. The information of the 6-axis force sensor is shown in Table IV, and the influence of different numbers of rubber strips on the friction force at different rotation speeds was determined. Moreover, the influence of different numbers of rubber strips on the hydrodynamic performance and torque was tested using computational fluid dynamics. The research results are presented in Fig. 7(a) and (b). According to the test results shown in Fig. 7(c), as the speed increases at the same number of rubber strips, the friction force monotonous decreases when the speed is less than 43 rpm. The friction force decreases by approximately 10%–20% when the speed is increased from 21.5 rpm to 43 rpm. In the presence of rubber strips, the friction force is considerably higher than that in the absence of rubber strips. The friction force maximum increase is approximately 300% at the same speed. When the number of rubber strips is greater than three, the increasing trend of the friction force gradually decreases, likely because all the rubber strips cannot simultaneously contact the ground. We can consider that the friction force monotonically increases as the number of rubber strips increases. When the number of rubber strips is less than six, the maximum changes in friction, torque, and thrust are about 170%, 9%, and 10.46%, respectively. These indicators of torque and thrust do not show obvious trends, and the changes are considerably smaller than the change in friction. Therefore, we can consider that the influence of the number of rubber strips on the hydrodynamic performance under this scheme can be ignored.

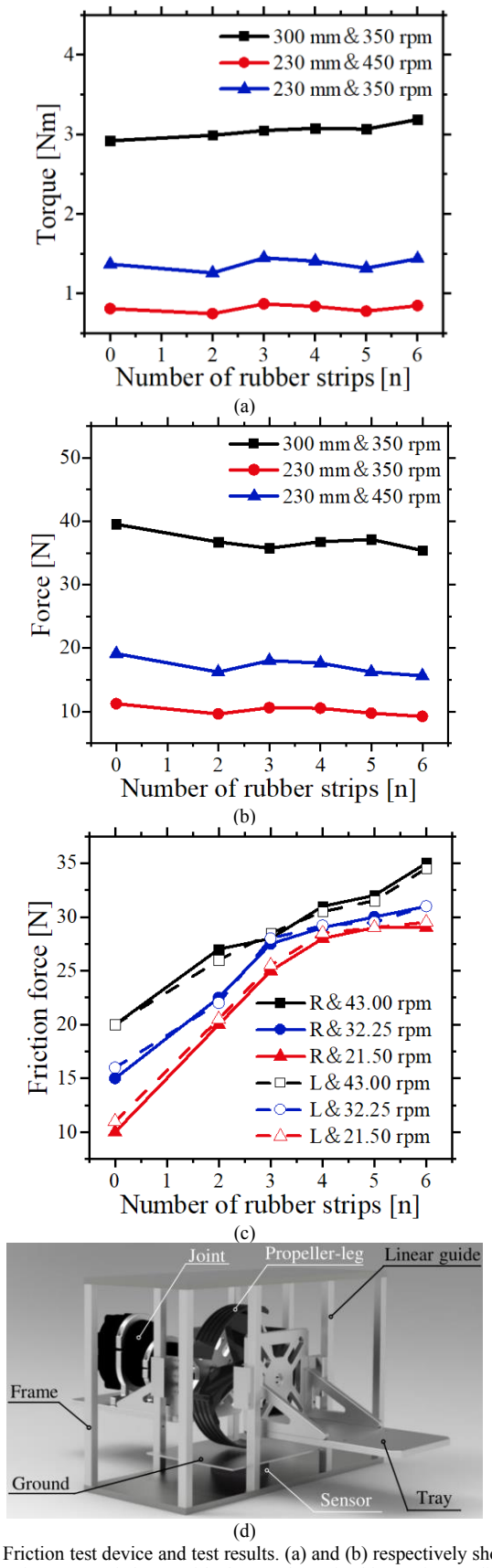

Fig. 7 Friction test device and test results. (a) and (b) respectively show the change of torque and thrust with the number of rubber strips at different speeds and diameters of propeller-leg. (c) shows the change of friction force with the rotate-speed and the number of rubber strips, (d) shows the test equipment.

TABLE IV
THE INFORMATION OF FORCE SENSOR

Parameter	Value	Unit
Sensor	SRI-M4325k1	/
Fx	200	N
Fy	200	N
Fz	400	N
Mx	20	Nm
My	20	Nm
Mz	20	Nm
Crosstalk	2.5	%F. S
Non-linearity	0.5	%F. S
Hysteresis	0.5	%F. S
Free air resinant freq	1500	Hz

III. MODELING OF THE SHOALBOT

A. Modeling and Control of the Running Mode

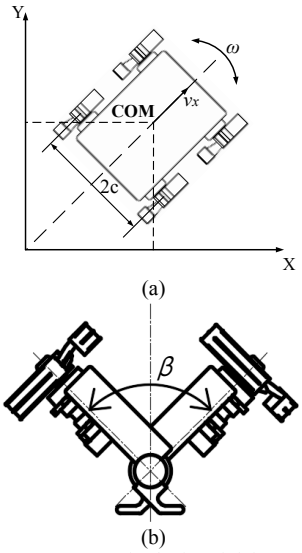

Fig. 8 (a) shows the SHOALBOT in the inertial frame when running. COM is the SHOALBOT's center of mass, v_x and ω are the linear and angular velocities, $2c$ is the distance between the left and right propeller-legs. (b) shows the SHOALBOT folds to angle β.

As shown in Fig. 8, COM is the SHOALBOT's center of mass. When the robot moves in the water, the buoyancy configuration makes the center of mass of the robot as close as possible to this point. Of course, the actual center of mass does not completely coincide with the geometric center. This is a simplification of the model. The kinematic model of SHOALBOT is based on the model proposed by Kozowski [25]. The inertial and body frames are presented in Fig. 7, and the relationship between the center of mass and angular velocities of the propeller-leg can be obtained:

$$\varepsilon = \begin{bmatrix} v_x \\ \omega \end{bmatrix} = r \begin{bmatrix} (\omega_L + \omega_R)/2 \\ (-\omega_L + \omega_R)/2 \end{bmatrix}. \quad (1)$$

where ε is a control input introduced at the kinematic level, i.e., the differential drive model of SHOALBOT. When the speeds on both sides of SHOALBOT are different, it runs in an arc trajectory. v_x and ω are the linear and angular velocities, and the radius of the arc trajectory is v_x/ω. r is the radius of the propeller-leg, ω_L and ω_R are the angular velocities of the left and right propeller-legs, respectively, and $2c$ is the distance between the left and right propeller-legs.

Unlike ordinary four-wheeled vehicles, SHOALBOT is a

robot with deformability, the original model cannot be directly applied to motion control. The variables c' and β are introduced. When the body folds to angle β, we replaced c with c' and $c' = c\cdot\sin(\beta/2)+r\cdot\cos(\beta/2)$ if $\beta \le \pi$, or $c' = c\cdot\sin(\pi-\beta/2)-r\cdot\cos(\pi-\beta/2)$ if $\beta > \pi$.

The trajectory of SHOALBOT can be observed as an arc. Walking in a straight line can be regarded as an infinite turning radius, and turning in place implies that the robot's turning radius is zero. Thus, the control variable ε can be provided as an input to the differential drive model to control SHOALBOT's movements. In theory, β, ω_L and ω_R can be used as motion control input signals such as v_x and ω (where the parameters r and c are known).

The dynamic model of SHOALBOT in the running mode uses Lagrangian dynamics [26]. The three 1-DOF legs are evenly distributed; hence, the kinetic and potential energy terms should be multiplied by three. The gait during the running mode includes bounding (simultaneous four-feet pedaling on the ground) and trotting (diagonal gait). The gravity term value is larger in the trotting gait than in the bounding gait. When calculating the maximum torque, the gravity and external force terms are calculated based on the trotting gait. The vector-matrix form as follows, where $\mathrm{M}(\theta)$ is the 3 × 3 inertia matrix of the leg, $\mathrm{H}(\theta,\dot{\theta})$ and $\mathrm{G}(\theta)$ are 3 × 1 vectors of centrifugal/Coriolis and gravitational forces/torques, respectively, τ_i is the 3 × 1 vector of joint torques and F_i is the 3 × 1 vector of ground reaction forces of the i-th foot. θ, $\dot{\theta}$, $\ddot{\theta}$ are the angle, angular velocity, and angular acceleration of joint.

$$\tau_i = [\mathrm{M}(\theta)]_i[\ddot{\theta}]_i + [\mathrm{H}(\theta,\dot{\theta})]_i + [\mathrm{G}(\theta)]_i - \mathrm{J}_i{}^{\mathrm{T}}\mathrm{F}_i. \quad (2)$$

B. Modeling and Control of the Swimming Mode

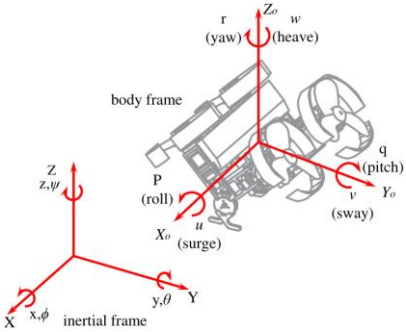

Fig. 9 SHOALBOT in the inertial and body frames when swimming. All the parameters are defined separately for the swimming mode, which is different from the meaning of the symbols in the previous paragraph. For example, θ here means the pitch angle and η means the attitude angle.

6-DOF parameters are needed when describing SHOALBOT's motion characteristics in the swimming mode (Fig. 9). There are four active degrees of freedom and two passive degrees of freedom, SHOALBOT does not have the ability to move horizontally in the X_0 and Y_0 directions. The position $\eta_1 = [x\ y\ z]^T$ and attitude angle $\eta_2 = [\phi\ \theta\ \psi]^T$ are defined in the inertial frame, where ϕ, θ, and ψ are the roll, pitch, and yaw angles, respectively. The linear velocities $v_1 = [u\ v\ w]^T$ and $v_2 = [p\ q\ r]^T$ are defined in the body frame, where u, v, and w are the velocities of the surge, sway, and heave, respectively, and p, q, and r are the angular velocities of roll, pitch, and yaw, respectively. The position and attitude angle can be described as $\eta = [x\ y\ z\ \phi\ \theta\ \psi]^T$, and the linear and angular velocities can be described as $v = [u\ v\ w\ p\ q\ r]^T$. Note that η is described in the inertial frame and v is described in the body frame.

The position and attitude angle information of SHOALBOT are measured using magnetic compasses here, and they exist in the earth frame. In contrast, the controller is designed according to the body frame. Moreover, the SHOALBOT's posture must be calculated based on the control force and torque. When the parameters are equal, converting the control force and movement in the body frame to those in the earth frame is necessary. Thus, the Euler angle is used to describe the SHOALBOT's posture in the earth frame. For the linear velocity,

$$\dot{\eta_1} = J_1(\eta_1)v_1\ . \quad (3)$$

where $J_1(\eta_1)$ is the conversion matrix of the line speed v_1 from the body frame to the earth frame:

$$J_1(\eta_1) = \begin{bmatrix} (\cos\theta\cos\psi\ -\sin\psi\cos\phi + \\ \cos\psi\sin\theta\sin\phi\ \sin\psi\sin\phi + \cos\psi\cos\phi\sin\theta) \\ (\sin\psi\cos\theta\ \cos\psi\cos\phi + \\ \sin\phi\sin\phi\sin\psi\ -\cos\psi\sin\phi + \sin\theta\sin\psi\cos\phi) \\ -\sin\theta\ \cos\theta\sin\phi\ \cos\theta\cos\phi \end{bmatrix}. \quad (4)$$

For the angular velocity,

$$\dot{\eta_2} = J_2(\eta_2)v_2. \quad (5)$$

where $J_2(\eta_2)$ is the conversion matrix of the angular velocity from the body frame to the earth frame:

$$J_2(\eta_2) = \begin{bmatrix} 1 & \sin\phi\tan\theta & \cos\phi\tan\theta \\ 0 & \cos\phi & -\sin\phi \\ 0 & \sin\phi\sec\theta & \cos\phi\sec\theta \end{bmatrix}. \quad (6)$$

Thus, the kinematic model of SHOALBOT in the swimming mode is,

$$\dot{\eta} = \begin{bmatrix} J_1(\eta_1) & 0_{3\times3} \\ 0_{3\times3} & J_2(\eta_2) \end{bmatrix}\begin{bmatrix} v_1 \\ v_2 \end{bmatrix} = J(\eta)v. \quad (7)$$

$J_2(\eta_2)$ will be meaningless when $\theta = \pm 90^\circ$, and $J_2(\eta_2) \neq J_2^T(\eta_2)$. As the Euler angle mainly equals $\pm 90^\circ$ in the swimming mode, using quaternions is necessary to represent the kinematic model of SHOALBOT if $\theta = \pm 90^\circ$ is included, which is not described in detail here.

The body folds to angle β in the swimming mode. Hence, the dynamic model at this time is expressed as

$$\tau_x = K = bl_x(\Omega_4^2 + \Omega_3^2 - \Omega_1^2 - \Omega_2^2)\,sin(\beta) - J\,sin(\beta)\dot{\theta}(-\Omega_4 + \Omega_3 + \Omega_1 - \Omega_2) \quad (8a)$$

$$\tau_y = M = bl_y(-\Omega_2^2 - \Omega_3^2 + \Omega_1^2 + \Omega_4^2)\,sin(\beta) + d(\Omega_2^2 + \Omega_3^2 - \Omega_1^2 - \Omega_4^2)\,cos(\beta) + J\,sin(\beta)\dot{\phi}(-\Omega_4 + \Omega_3 + \Omega_1 - \Omega_2) \quad (8b)$$

$$\tau_z = N = bl_y(\Omega_4^2 + \Omega_2^2 - \Omega_3^2 - \Omega_1^2)\,cos(\beta) + d(-\Omega_4^2 - \Omega_2^2 + \Omega_3^2 + \Omega_1^2)\,sin(\beta) + J\,cos(\beta)\dot{\phi}(-\Omega_4 + \Omega_3 - \Omega_1 + \Omega_2) \quad (8c)$$

$$F_x = 0 \quad (9a)$$

$$F_y = b(\Omega_1^2 + \Omega_2^2 - \Omega_3^2 - \Omega_4^2)\,cos(\beta) \quad (9b)$$

$$F_z = b(\Omega_1^2 + \Omega_2^2 + \Omega_3^2 + \Omega_4^2)\,sin(\beta) \quad (9c)$$

where b is the propeller-leg propulsion efficiency, d is the propeller-leg drag efficiency, and Ω_i is the rotate-speed of the i-th propeller-leg.

To obtain the state parameters of each propeller-leg in the robot's complex trajectory swimming process, according to the swimming movement model, the SHOALBOT spatial multi-degree-of-freedom swimming simulation environment is established according to the PID control theory, in which the hydrodynamic coefficients are measured according to the method and definition in [27]， and shown in TABLE V. We adjust the input parameters (Yaw, Pitch and Roll) of the robot motion process in the simulation environment, and the output of the simulation is the motion trajectory. We adjust the input parameters to get the desired motion trajectory (including straight line, turning, circular trajectory and helical trajectory), and use the input parameters debugged in the simulation as the input of the robot motion control to conduct swimming tests. In the simulation environment, set the rectangular swimming trajectory that 4 m × 6 m, circular swimming trajectory with a radius of 3m and the spiral swimming trajectory with a radius of 3m and a pitch of 1m, and get the parameters, applying them to the performance test of the robot has verified that this kind of structural scheme of SHOALBOT has the ability to swim in space with multiple degrees of freedom. The code of the simulation environment and simulation data of the simulation trajectory is uploaded as an attachment. The SHOALBOT swam according to the state parameters obtained by the simulation, and the figures of the swimming trajectory and the simulation trajectory are shown in the experimental part.

TABLE V
INFORMATION OF MAIN HARDWARE OF THE CONTROL SYSTEM

Parameter	Value	Parameter	Value
I_{xx}	7.334 Nm^2	$X_{\dot{u}}$	-13.75 Ns^2/m
I_{yy}	3.934 Nm^2	$Y_{\dot{v}}$	-16.5 Ns^2/m
I_{zz}	5.390 Nm^2	$Z_{\dot{w}}$	-48 Ns^2/m
X_u	-1.425 Ns/m	$K_{\dot{p}}$	-29.85 Nms^2/rad
Y_v	-6.613 Ns/m	$M_{\dot{q}}$	-35.82 Nms^2/rad
Z_w	-3.16 Ns/m	$N_{\dot{r}}$	-30.25 Nms^2/rad
$X_{\|u\|u}$	-35.2 Ns^2/m^2	z_G	-0.1 m
$Y_{\|v\|v}$	-41.852 Ns^2/m^2	z_B	-0.2 m
$Z_{\|w\|w}$	-31.6 Ns^2/m^2		

IV. EXPERIMENT

We using a KOLLMORGEN TBM(S)-6013-A motor with a gearbox of a 6.3 reduction ratio, the theoretical maximum torque can reach 7.5 Nm. When the transmission efficiency of the planetary reducer is multiplied by a coefficient of 0.9, the output torque can reach 6.75 Nm to meet the running demand. At this time, the peak speed of the joint output is 682.5 . Based on the hydrodynamic simulation analysis results, a single propeller-leg can produce a thrust of approximately 30 N under the condition of 600 rpm. When the folding angle of the body is 90°, the four propeller-legs can produce a thrust of ~84 N. The net buoyancy of the designed robot in water is 50 N, meeting the design requirements. The structural design of the joint is depicted in Fig. 10. Unlike those of conventional underwater propellers, the joints of the propeller-leg propulsion device receive a large radial impact load during the running motion; hence, a sealing treatment is required at the output shaft.

According to kinetic calculations, when SHOALBOT is running or swimming, the maximum torque received by the deformable joint is 35 Nm. The deformable joint uses a KOLLMORGEN TBM(S)-6013-A motor with a harmonic deceleration device with a 100-time reduction ratio.

All joints adopt an integrated modular design. In other words, the gearbox, motor, encoder, and driver are integrated into a set of shells for unified sealing. All energy supply and communication are completed internally, relying on the interaction of power and communication lines with the control box.

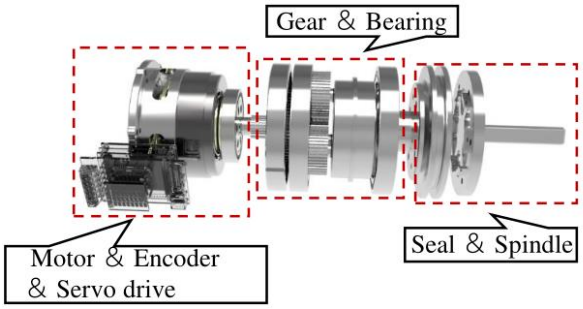

Fig. 10 Drive joint of SHOALBOT. All parts of the joint are integrated into a waterproof shell, and the output shaft is sealed.

The hardware's layout of the SHOALBOT's control system is shown in Table VI, where the data collected using the depth sensor and magnetic compass are fed back to the upper computer PC104 for processing. Then, the control instructions are sent to STM32f103C8T6 for motion control. The entire energy supply of the robot relies on a lithium battery integrated in the robot's body.

TABLE VI
INFORMATION OF MAIN HARDWARE OF THE CONTROL SYSTEM

Equipment	Type	
Auxiliary control system		
Energy	Lithium battery	
Magnetic compass	NVA40-GPS/MINS	Sensor and
Depth sensor	miniIPS	power
Power system	Transformer	
Computers		
Embedded computer	PC104	CPU
Microcontroller unit	STM32f103C8T6	

To demonstrate the multimode movements in the amphibious environments, we carried out a series of performance demonstration experiments. The attribute of SHOALBOT can be seen in Table VII.

TABLE VII
THE ATTRIBUTE OF SHOALBOT

Attribute	Value
Body Height (mm)	220
Overall Width (mm)	500
Body Length (mm)	600
Leg to Leg Spacing (mm)	395
Ground Clearance (mm)	33
Inverted Ground Clearance (mm)	10
Leg Diameter (mm)	220
Total Weight (kg)	22

A. *Experiments of Running on the Beach*

We evaluated the performance of the SHOALBOT when running on the beach and compared the forward and reverse running modes, pedal the ground with the heel first when running forward, and pedal the ground with the toe first when running reverse. The SHOALBOT was unloaded during the experiment, the speed of the input command is 180 rpm for each joint. We completed five repeated tests on each of the two running modes in the same period and the same area (8 m × 8 m), the trajectory of each experiment does not involve the previously exercised area. We cannot find ten identical beach environments to ensure that the experimental conditions are completely consistent. In this way, can guarantee the similarity of experimental conditions. Calculate the linear velocity of the SHOALBOT by recording the position information of the robot in a fixed time interval. To measure the position, a local positioning system (UWB Mini 3, TREK 1000, including 4 base stations and 1 tag, positioning accuracy error $\leqslant$ 150 mm，communication distance $\geqslant$ 50 m) is used, the tag was placed at the front geometric center of the robot. The attitude control relies entirely on the onboard feedback from the single IMU residing on the control module. The remote control (RC) is used to initiate and terminate the running by wireless communication, and the ground station records the position information from UWB.

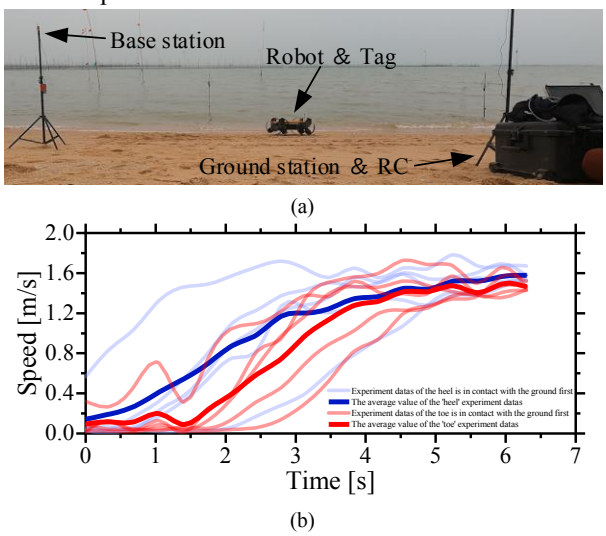

Fig. 11 Comparison of the running speed of the propeller-leg pedaling on the ground in different ways. (a) shows the testing process, and (b) shows the test data.

Fig. 11 shows sample data acquired in this experiment. From the average results of all tests, the average speed of forwarding motion is better than that of reverse motion, the difference of maximum speed is ~10.82%. This may be because the toes are sharper and sink deeper into the sand during running, resulting in a greater loss of movement speed.

B. *The Measurement Set-up of Swimming Experiments in the Pool*

SHOALBOT's swimming experiment data in the pool are all from sensors. The data of angle is obtained from the IMU (NAV40) that was placed on the body of the robot, the accuracy of attitude angle (Roll and Pitch) is $\leqslant$ 0.5° when static and $\leqslant$ 1.0° when moving, the accuracy of heading angle (Yaw) is $\leqslant$ 2.0° . The collection of the SHOALBOT's depth information relies on a depth sensor (miniIPS, range from 0 bar to 5 bar, and the accuracy is 0.01%) that was placed on the back of the robot, and the probe position is at the geometric center of the robot's back. Each joint has an encoder (RLS MRA029BC010DSE00, 17 bits, from 0.4 MHz to 5 MHz, communication interfaces is BISS-C) set to record the rotate-speed of the propeller-leg. The set-up of the sensors are shown in Fig. 12.

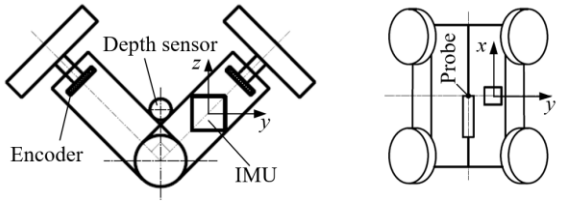

Fig. 12 The set-up of the sensors. The encoder measures the rotational speed of the Propeller-leg, the probe position is at the geometric center of the robot's back, *x*, *y*, and *z* is the coordinate definition of the IMU.

C. *Experiments of Swimming in the Pool*

First, the entire process experiment of bottom-running, mode switching, swimming, and hovering was carried out at the dock (3 m × 3 m × 5 m), depth of the dock is 3 m, and then the SHOALBOT's spatial multi-degree-of-freedom swimming experiment was carried out in the test pool (10 m × 50 m × 30 m), depth of the pool is 10 m.

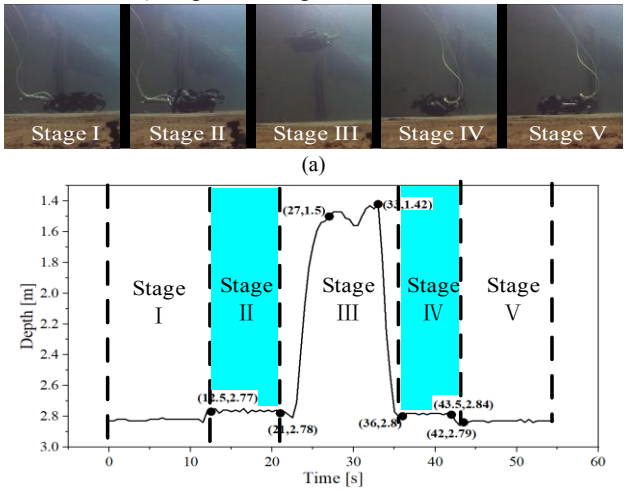

Fig. 13 SHOALBOT's movement mode switching process in the water. Stage I is running, Stage II is deforming to swimming mode, Stage III is swimming and hovering, Stage IV is falling back to the bottom and deforming to running mode, Stage V is running. The blue area is the SHOALBOT's deformation and mode switching phase (see video).

The entire process is shown in Fig. 13, includes five stages. Stage I is the running stage, the distance between the depth sensor and the bottom at this time is 0.15 m according to the structure of the robot. Then the SHOALBOT deformed and switched the move-mode in Stage II, the data of the depth sensor has changed ~0.06 m. The SHOALBOT swam away from the bottom of the pool and hovering at about 1.5 m below the water surface for 6 s and then fell back to the

bottom during Stage III. Finally, the SHOALBOT deformed and switched back to running mode in Stage IV and Stage V. The data example of Fig. 13 was all recorded by the depth sensor, and the sensor was calibrated before the experiment. The entire process experiment proved that the SHOALBOT can running at the bottom of the pool and swimming in the water, and switching between different move-modes.

A hovering experiment was carried out to prove the SHOALBOT can adjust its posture in the water, and the data examples of encoder and IMU are shown in Fig. 14, it can be seen that when the attitude angle changes, each propeller-leg can adjust the rotate-speed accordingly to correct the error angle of the body, the roll angle during the entire hovering process is guaranteed to be less than ± 5°, this is consistent with the indicators we set in the control program. The results show that SHOALBOT can achieve stable hovering after several adjustments during the swimming process.

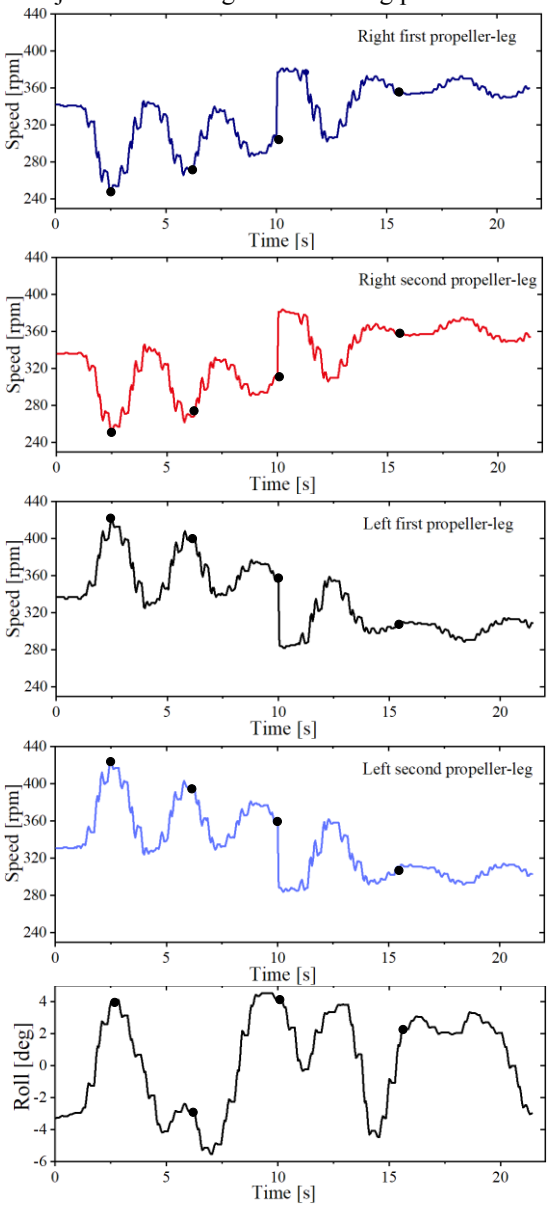

Fig. 14 Changes in the rotate-speed of the four propeller-legs and the roll angle of the SHOALBOT during hovering, each solid circle in the curve represents one time of posture adjustment.

We calculate the position coordinates of the robot according to the depth, the rotation speed of the propeller-leg, and the angle information recorded by the depth gauge, encoder and IMU carried by the SHOALBOT. The linear speed of the robot in all directions can be calculated based on the rotation speed of propeller-leg and angle information as shown in Fig. 9, and we record the speed and depth information of the robot at a frequency of 20Hz to fit the trajectory of the robot.

Fig. 15 shows the data examples of actual trajectory and simulation trajectory. SHOALBOT swam on a rectangular trajectory that 4 m × 6 m with a fixed 2m-depth below the water surface, and swam on a circular trajectory with a radius of 3 m in a two-dimensional plane with a fixed 0.5m-depth below the water surface and completed the spiral trajectory swimming in the three-dimensional space from the depth of 0.5m to 2.5m. The swimming experiments in the pool prove that although the SHOALBOT lacks two active degrees of freedom, the structural scheme still can swim in space with multiple degrees of freedom, and can complete complex trajectory movements in three-dimensional space.

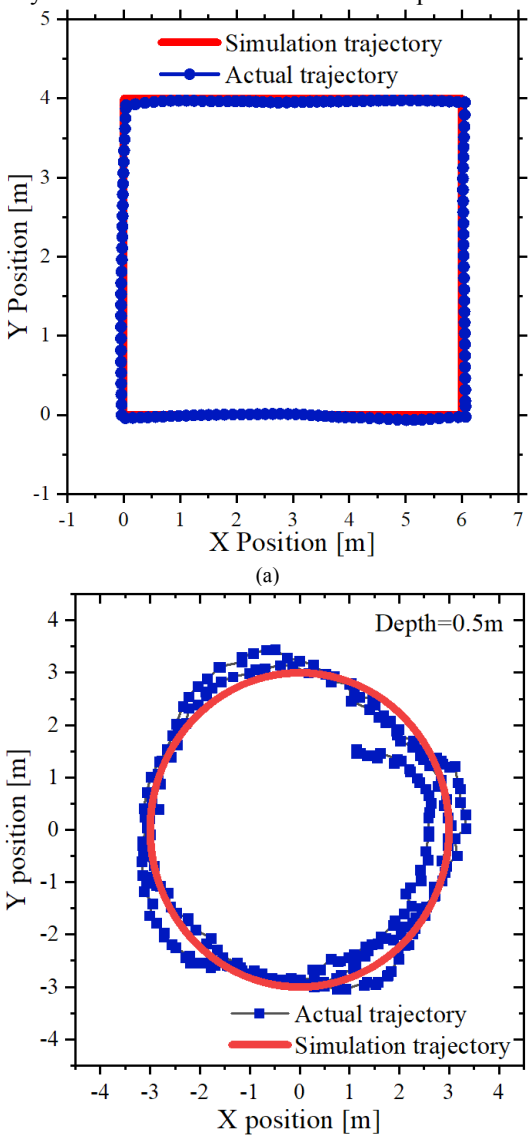

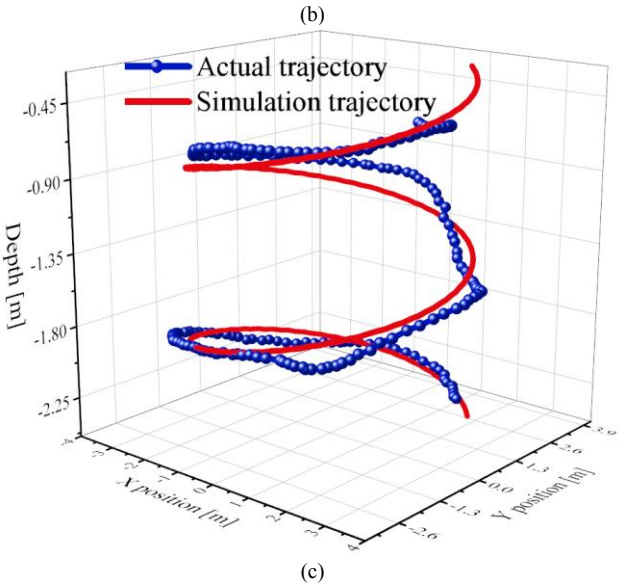

Fig. 15 (a) SHOALBOT swimming on rectangular path, (b) SHOALBOT swimming on circular path and (c) SHOALBOT swimming on radius path. The red and blue lines represent the simulation trajectory and the actual movement trajectory, respectively (see video).

D. Experiments of Functional Verification

Fig. 16 The SHOALBOT successfully running over different challenging surfaces including turf, slope, dry sand, wet sand, and bottom of the pool (see video).

The SHOALBOT was tested outdoor running over different surfaces. In Fig. 16, the SHOALBOT is shown running over different surfaces including turf, slope, dry sand, wet sand, and bottom of the pool (depth-10 m). SHOALBOT carried a payload of 9 kg (~0.4 body weight), ran a distance of 30 m in 25 s on naturally formed soft turf, and achieved a linear speed of 1.2 m/s (~2 body lengths/s). Then SHOALBOT was operated in a real seaside environment to verify its running ability. Based on the previous experiment, we widened the foot in an attempt to improve its running ability. The experiment performed on a completely soft horizontal dry beach proved that when the foot width was doubled, the robot ran a distance of 20 m in only 12 s. Moreover, the highest running speed was approximately 3 body lengths/s (1.8 m/s). This proves that the geometric parameters of the robot can be locally improved according to the actual situation to enhance its motion abilities in a certain environment. Similarly, the robot with the widened foot could reach a running speed of nearly 2.5 body lengths/s (1.5 m/s) on a wet beach.

After successfully testing the running ability, SHOALBOT carried a 9 kg payload and climbed up the steps with a height of 100 mm (~0.4 body height), as shown in video, this reflects the superiority of the feet over wheels.The SHOALBOT crawled on the seabed in shallow waters at the land-water junction, the experimental results proved that the robot could switch from land to sea environments and crawl on the extremely soft sandy seabed as shown in video.

The moving speed of the SHOALBOT in the water is measured in a pool, where the running speed is measured by running from one edge to the other edge in a pool of fixed width (3m) and recording the passing time, the running speed at the bottom of the pool can reach 0.5m/s. The swimming speed is measured by the length of the rope dragged by the robot's tail, and the swimming speed in the pool can reach 1m/s. The currents in some movement modes are shown in the TABLE VIII, and the measurement method and data are shown in the attachment.

TABLE VIII
CHARACTERISTICS OF THE AMPHIBIOUS ROBOTS, WHICH INCLUDES THE MASS, DIMENSIONS, AND SPEED

	Movement mode	Current	Performance parameters
1	Running on sand	1.28 A	1 m/s
2	Running on turf	2.18 A	1 m/s
3	Running on gravel road	1.47 A	1 m/s
4	Swimming in a straight line	2.81 A	1 m/s
5	Hovering in the water	2.60 A	

Using only the simplest control method, numerous experimental results show that the propeller-leg amphibious robot obtained using the optimized design method can adapt to various typical environments at the land–water junction and exhibit strong terrain-passing and flexible swimming abilities.

Compares with some robots of the same size and type that have been published [28], and the comparison results are shown in Table IX. It can be seen that SHOALBOT performs well in terms of multi-modality and athletic ability in the amphibious environment. Although some robots are faster than SHOALBOT, the amphibious environment that these robots can cover is not as comprehensive as SHOALBOT. Among the robots that can completely cover the entire environment from land to sea (including land, water, and bottom), SHOALBOT's speed is the fastest (include only publicly available information), of course, it also has the

ability of climbing (100mm, ~0.43 body height) and loading (9kg, ~0.4 body weight).

TABLE IX
CHARACTERISTICS OF THE AMPHIBIOUS ROBOTS, WHICH INCLUDES THE MASS, DIMENSIONS, AND SPEED

Name	Mass (kg)	Dimensions (L × W × H) (mm)	Top Speed (mm/s)	Top Speed (bodylengths/s)	Covering Environment		
					Land	Water	Bottom of the sea
SHOALBOT (2021)	**22**	**600 × 500 × 220**	**1800 (on land), 1000 (underwater)**	**3 (on land), 1.67 (underwater)**	√	√	√
MiniTurtle-I (2012)	5	310 × 530 × 200	3 (on land), 150 (underwater)	0.0097 (on land), 0.48 (underwater)	√	√	√
ForBot (2015)	13	700 × 260 × 230	470 (on land), 400 (underwater)	0.67 (on land), 0.57 (underwater)	√	√	√
Soft-amphibious robot (2017)	0.07	210 × 210 × 50	56 (on land), 22 (underwater)	0.27 (on land), 0.105 (underwater)	√	×	√
AmphiHex-II (2018)	14	510 × 330 × 100	350 (on land), 180 (underwater)	0.69 (on land), 0.35 (underwater)	√	√	√
Turtle-inspired robot (2019)	9.4	NA	53 (on land), 35 (underwater)	NA, NA	√	√	√
AmphiSTAR (2020)	0.246	265 × 265 × NA	3600 (on land), 1500 (on water)	13.58 (on land), 5.66 (on water)	√	√	×
Velox	NA	NA	NA (on land), NA (underwater)	NA (on land), NA (underwater)	√	√	√
Whegs IV (2005)	14.5–15.5	NA	NA	NA	√	√	√
AQUA (2007)	16	650 × 450 × 130	1000 (underwater)	1.54 (underwater)	×	√	×
X-RHex (2010)	8.6–9.5	570 × 390 × 75	1540 (on land)	2.7 (on land)	√	×	√
Ninja Legs (2013)	16-18	NA	900 (on land)	NA	√	√	√

V. CONCLUSION

This study proposes a new type of amphibious robot. The robot is equipped with only one type of propulsion device, and this combined with the deformability of the robot's body enables it to work on land and in water. Such a structure facilitated the design of the miniature and lightweight robot, alleviating the problem of additional energy consumption owing to the mutual load of various propulsion devices when they are used alone.

The combination of the blade and foot and the geometric parameters of each component influence the running and swimming abilities of the robot. Thus, we proposed a robot design and optimization method, combined with theoretical calculations, experiments, and simulations, to optimize the design of the propeller-leg propulsion device.

We fabricated the amphibious robot and verified its running and swimming abilities in a simulated experimental site and typical natural environment to demonstrate its feasibility. Experimental results proved that the robot could reach a running speed of ~2 body lengths/s under a load of 0.4 times its own weight on turf. Furthermore, it could achieve a running speed of ~2 body lengths/s under no-load conditions on soft and dry sand; after partial improvements in its feet, it could reach a running speed of ~3 body lengths/s. The experiment conducted in the pool showed that SHOALBOT could operate at a depth of 10 m and float under 50-N net buoyancy. It exhibited spatial motion abilities in the water, including depth and direction fixation, direct flight, and autonomous movement based on a predefined spiral trajectory with multi degrees of freedom.

VI. ACKNOWLEDGMENT

The authors would like to thank X. Chen from Heilongjiang Institute of Technology for the support on experiment, and G. C. Zhang for the support on control system design and the assistance in PCB board design.

REFERENCES

[1] M. Zhou, R. Bachmayer, B. Deyoung, "Mapping the underside of an iceberg with a modified underwater glider," *Journal of Robotic Systems*, vol. 36, no. 6, pp. 1102-1117, Sep. 2019, 10.1002/rob.21873.

[2] M. Kalaitzakis, B. Cain, N. Vitzilaios, I. Rekleitis, J. Moulton, "A marsupial robotic system for surveying and inspection of freshwater ecosystems," *Journal of Field Robotics*, vol. 38 no. 1 pp. 121-138, Jan. 2021, 10.1002/rob.21957.

[3] J. Das, F. Py, J. B. J. Harvey, J. P. Ryan, A. Gellene, R. Graham, D. A. Caron, K. Rajan, G. S. Sukhatme, "Data-driven Robotic Sampling for Marine Ecosystem Monitoring," *International Journal of Robotics Research*, vol. 34, no. 12, pp. 1435-1452, Oct. 2015, 10.1177/0278364915587723.

[4] D. R. Yoerger, A. M. Bradley, B. B. Walden, M. H. Cormier, W. B. F. Ryan, "Fine-Scale Seafloor Survey in Rugged Deep-Ocean Terrain with an Autonomous Robot," *IEEE International Conference on Robotics & Automation*, Apr. 2000, pp. 1787-1792, 10.1109/ROBOT.2000.844854.

[5] O. B. Humborstad, L. Nottestad, S. Lokkeborg, H. T. Rapp, "RoxAnn bottom classification system, sidescan sonar and video-sledge: spatial resolution and their use in assessing trawling impacts," *ICES Journal of Marine Science*, vol. 61, no. 1, pp. 53-63, Feb. 2004, 10.1016/j.icesjms.2003.10.001.

[6] H. Singh, T. Maksym, J. Wilkinson G. Williams, "Inexpensive, small AUVs for studying ice-covered polar environments," *Science Robotics*, vol. 2, no. 7, Jun. 2017, 10.1126/scirobotics.aan4809.

[7] N. Mazouchova, N. Gravish, A. Savu D. I. Goldman, "Utilization of granular solidification during terrestrial locomotion of hatchling sea turtles," *Biology Letters*, vol. 6, no. 3, pp. 398-401, Jun. 2010, 10.1098/rsbl.2009.1041.

[8] Z. E. Teoh, B. T. Phillips, K. P. Becker, G. Whittredge, J. C. Weaver, C. Hoberman, D. F. Gruber, R. J. Wood, "Rotary-actuated folding polyhedrons

for midwater investigation of delicate marine organisms," *Science Robotics*, vol. 3, no. 20, Jul. 2018, 10.1126/scirobotics.aat5276.
[9] Y. W. Huang, Y. Sasaki, Y. Harakawa E. F. Fukushima, S. Hirose, "Operation of underwater rescue robot anchor diver III during the 2011 Tohoku Earthquake and Tsunami," *OCEANS'11 MTS/IEEE KONA*, 2011, 10.23919/OCEANS.2011.6107198.
[10] N. A. Cruz, A. C. Matos, "The MARES AUV, a Modular Autonomous Robot for Environment Sampling," *OCEANS 2008*, 10.1109/OCEANS.2008.5152096.
[11] H. Greiner， A. Shectman， C. Won， R. Elsley， P. Beith, "Autonomous legged underwater vehicles for near land warfare," *Proceedings of Symposium on Autonomous Underwater Vehicle Technology*, pp. 41-48, June, 1996, 10.1109/AUV.1996.532399.
[12] G. Dudek， P. Giguere， C. Prahacs S. Saunderson, J. Sattar, L. A. Torres-Mendez, M. Jenkin, A. German, A. Hogue, A. Ripsman, J. Zacher, E. Milios, H. Liu, P. Zhang, M. Buehler, C. Georgiades, "AQUA: An Amphibious Autonomous Robot," *Computer*, vol. 40, no. 1, pp. 46-53, Jan. 2007, 10.1109/MC.2007.6.
[13] R. Altendorfer, N. Moore, H. Komsuolu M. Buehler, H. B. Brown, D. McMordie, U. Saranli, R. Full, D. E. Koditschek, "RHex: A Biologically Inspired Hexapod Runner," *AUTONOMOUS ROBOTS*, vol. 11, no. 3, pp. 207-213, Nov. 2001, 10.1023/A:1012426720699.
[14] U. Saranli, M. Buehler, D. E. Koditschek, "RHex: A simple and highly mobile hexapod robot," *INTERNATIONAL JOURNAL OF ROBOTICS RESEARCH*, vol. 20, no. 7, pp. 616-631, Jul. 2001, 10.1177/02783640122067570.
[15] P. C. Lin, H. Komsuoglu, D. E. Koditschek, "Sensor Data Fusion for Body State Estimation in a Hexapod Robot With Dynamical Gaits," *IEEE Transactions on Robotics*, vol. 22, no. 5, pp. 932-943, Oct. 2006, 10.1109/TRO.2006.878954.
[16] J. C. Spagna, D. I. Goldman, P. C. Li. D. E. Koditschek, R. J. Full, "Distributed mechanical feedback in arthropods and robots simplifies control of rapid running on challenging terrain," *Bioinspiration & Biomimetics*, vol. 2, no. 1, pp. 9-18, Mar. 2007, 10.1088/1748-3182/2/1/002.
[17] X. G. Song, X. L. Zhang, X. Y. Meng, C. J. Chen, "Gait optimization of step climbing for a hexapod robot," *JOURNAL OF FIELD ROBOTICS*, Sep. 2021, 10.1002/rob.22037.
[18] C. Georgiades, A. German, A. Hogue, H. Liu, C. Prahacs, A. Ripsman, R. Sim, L. A. Torres, P. Zhang, M. Buehler, G. Dudek, M. Jenkin, E. Milios, "AQUA: an aquatic walking robot," *2004 IEEE/RSJ International Conference on Intelligent Robots and Systems (IROS)*, Oct. 2004, 10.1109/IROS.2004.1389962.
[19] G. Dudek, M. Jenkin, C. Prahacs, A. Hogue, J. Sattar, P. Giguere, A. German, H. Liu, S. Saunderson, A. Ripsman, S. Simhon, L. A. Torres, E. Milios, P. Zhang, I. Rekletis, "A visually guided swimming robot," *2005 IEEE/RSJ International Conference on Intelligent Robots and Systems (IROS)*, pp. 1749-1754, Aug. 2005, 10.1109/IROS.2005.1545231.
[20] B. B. Dey, S. Manjanna, G. Dudek, "Ninja Legs: Amphibious One Degree of Freedom Robotic Legs," *IEEE/RSJ International Conference on Intelligent Robots and Systems (IROS)*, Nov. 2013, pp. 5622–5628.
[21] Y. S. Kim, G. P. Jung, H. Kim, K. J. Cho, C. N. Chu, "Wheel transformer: A miniaturized terrain adaptive robot with passively transformed wheels," *2013 IEEE International Conference on Robotics and Automation (ICRA)*, pp. 5625–5630, May. 2013, 10.1109/ICRA.2013.6631385.
[22] Y. S. Kim, G. P. Jung, H. Kim, K. J. Cho, C. N. Chu, "Wheel Transformer: A Wheel-Leg Hybrid Robot With Passive Transformable Wheels," *IEEE Transactions on Robotics*, vol. 30, pp. 1487-1498, Nov. 2014, 10.1109/TRO.2014.2365651.
[23] X. Liang, M. Xu, L. C. Xu, L. Peng, X. S. Ren, Z. W. Kong, J. Yang, S. W. Zhang, "The AmphiHex: a Novel Amphibious Robot with Transformable Leg-flipper Composite Propulsion Mechanism," *2012 IEEE/RSJ INTERNATIONAL CONFERENCE ON INTELLIGENT ROBOTS AND SYSTEMS (IROS)*, pp. 3667-3672, Oct. 2012, 10.1109/IROS.2012.6386238.
[24] L. Bai, G. Z. Dou, W. B. Duan, Y. X. Sun, J. Zheng, X. H. Chen, "Amphibious Robot with a Novel Composite Propulsion Mechanism," *IEEE International Conference on Advanced Robotics and Mechatronics*, pp. 442-447, Jul. 2021.
[25] K. Kozowski, D. Pazderski, "Modeling and control of a 4-wheel skid-steering mobile robot," *International Journal of Applied Mathematics and Computer Science*, vol. 14, no. 4, pp. 477-496, 2004.
[26] S. S. Roy, D. K. Pratihar, "Kinematics, Dynamics and Power Consumption Analyses for Turning Motion of a Six-Legged Robot," *Journal of Intelligent & Robotic Systems*, vol. 74, no. 3-4, pp. 663-688, Jun. 2014, 10.1007/s10846-013-9850-6.
[27] T. Gao, Y. J. Pang, Y. X. Wang, Q. L. Chen, "Calculation method of hydrodynamic coefficients for underwater vehicles," *Journal of Harbin Engineering University*, vol. 40, no. 1, pp. 174-180, Jan. 2019, 10.11990/jheu.201709100.
[28] K. Ren, Yu. J, "Research status of bionic amphibious robots: A review," *Ocean Engineering*, vol. 227, May. 2021, 10.1016/j.oceaneng.2021.108862.

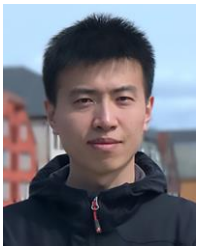

Gang Wang received the B.Eng. degree in Mechanical Design Manufacture and Automation from Harbin Engineering University in China in 2006. He also obtained the M.S. and Ph.D. degrees in Mechanical Engineering from Harbin Engineering University, China in 2008 and 2011 respectively.

He is currently working as an Associate Professor at the Science and Technology on Underwater Vehicle Laboratory of Harbin Engineering University and he also serves as an associate professor in the College of Shipbuilding Engineering, Harbin Engineering University. His research interests include the fields of intelligent robotic systems and underwater robotics.

Xinmeng Ma received the B.S. degree in Mechanical Design manufacture and Automation Major from Harbin Engineering University in China in 2016. He is currently working toward the Ph.D. degree in Mechanical Engineering.

His current research interests are mechanism design and optimization method for biological inspired legged locomotion, the motion method of legged robot on wet granular ground, co-simulation of the legged robot running on the granular media ground, amphibious multi-legged robot.

Kaixin Liu received the B.S. degree in Naval Architecture and Ocean Engineering from Harbin Engineering University in 2019, received the M.S degree in Naval Architecture and Ocean Engineering from Harbin Engineering University in 2022.

His current research interests are trajectory tracking control of underwater underactuated robots and dynamics modeling of underwater vehicles.